Graphene Synthesis and Its Recent Advances in Applications—A Review

Santhiran, A., Iyngaran, P., Abiman, P. & Kuganathan, K.

DOI 10.3390/c7040076
ESSN 2311-5629

Publisher: MDPI

C Journal of Carbon Research

MDPI

Review

Graphene Synthesis and Its Recent Advances in Applications—A Review

Anuluxan Santhiran [1], Poobalasuntharam Iyngaran [1], Poobalasingam Abiman [1] and Navaratnarajah Kuganathan [2,3,*]

[1] Department of Chemistry, University of Jaffna, Sir. Pon Ramanathan Road, Thirunelvely, Jaffna 40000, Sri Lanka; sanuluxan@gmail.com (A.S.); piyngs7@gmail.com (P.I.); abiman777@gmail.com (P.A.)
[2] Department of Materials, Imperial College London, London SW7 2AZ, UK
[3] Faculty of Engineering, Environment and Computing, Coventry University, Priory Street, Coventry CV1 5FB, UK
* Correspondence: n.kuganathan@imperial.ac.uk

Abstract: Owing to the remarkable chemical and physical properties, graphene has been widely investigated by researchers over the last 15 years. This review summarizes major synthetic methods such as mechanical exfoliation, liquid phase exfoliation, unzipping of carbon nanotube, oxidation-reduction, arc discharge, chemical vapor deposition, and epitaxial growth of graphene in silicon carbide. Recent advances in the application of graphene in graphene-based lithium ion batteries, supercapacitors, electrochemical sensors, transparent electrodes and environmental based remedies are discussed.

Keywords: graphene; chemical vapor deposition; supercapacitors; batteries; photocatalyst

Citation: Santhiran, A.; Iyngaran, P.; Abiman, P.; Kuganathan, N. Graphene Synthesis and Its Recent Advances in Applications—A Review. *C* **2021**, *7*, 76. https://doi.org/10.3390/c7040076

Academic Editors: Gil Goncalves and Stefano Bellucci

Received: 8 September 2021
Accepted: 8 November 2021
Published: 10 November 2021

1. Introduction

Graphene has been extensively studied by scientific and engineering communities for more than 15 years since its first fabrication reported in 2004 [1]. Graphene is a single layer of two-dimensional carbon atoms in a hexagonal lattice structure and has been widely used in many applications such as electronics [2], energy storing batteries [3], super capacitors [4], fuel cells [5] and solar cells [6,7] owing to its unique high surface area, thermal [8] and electrical conductivity [9] and mechanical strength [10]. Graphene is one of the allotropes of carbon and it is made of hexagons. Other allotropes include fullerenes (0D), nanotubes (1D) and graphite (3D) (see Figure 1). Graphene based nanomaterials include reduced graphene oxide, graphene quantum dots and graphene oxides. Graphene ideally consists of sp^2 carbon atoms but other family members comprise of sp^2 and sp^3 due to the introduction of the functional groups such as hydroxyl, carboxyl, carbonyl and epoxy groups [11].

Graphene consists of two-dimensional layer of carbon atoms with sp^2 hybridization arising from mixing of s, p_x and p_y orbitals. The remaining p_z orbital of each carbon atom forms π bonds with three neighboring carbon atoms, known as valence band and a band of empty π^* orbitals known as conduction band [12]. Carbon has four valence electrons, and three of them form sigma bonds that are back bone of hexagonal structure. The remaining electron forms one third of π bond with the nearest neighbor carbon atom. These out of plane interactions are extremely weak leading to out of plane electrical and thermal conductivities which are ~103 times lower than that of in plane analogues [13]. A single layer of graphene consists of hexagonal layer of carbon atoms. Bi-layer has 2 and few layer graphene has 3 to 10 layers of two-dimensional sheets. Graphene with more than 10 layers is known as thick graphene and has less scientific interest. In Bi- layer and few layer graphene, carbon atoms are stacked in different possible ways, hexagonal or AA stacking, Bernal or AB stacking and rhombohedral way or ABD stacking [14]. In a twisted bilayer graphene, layers are twisted at a small angle [15].

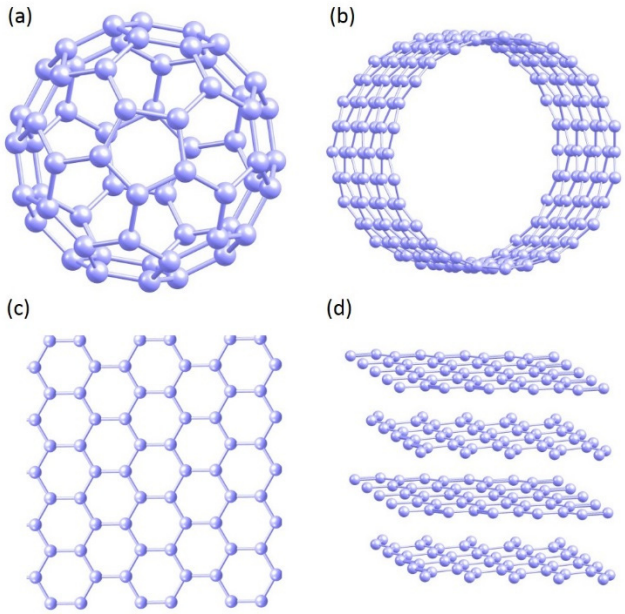

Figure 1. (**a**) Zero-dimensional Fullerene, (**b**) one-dimensional carbon nanotube (**c**) two-dimensional graphene and (**d**) three-dimensional graphite.

Graphene attracted great attention due to its excellent electronic properties. Graphene is a semiconductor with a small band gap [16]. The electron mobility of graphene at room temperature was found to be as high as 15,000 $cm^2V^{-1}s^{-1}$ with small temperature dependency and zero effective mass for the charge carriers [17]. In most of the materials, the electron movement is hindered by phonon scattering. However, in the case of graphene, the movement of electrons is hindered only by defect scattering. As a result, the theoretical limit of resistivity of graphene is estimated to be 10^{-6} Ω cm which is the lowest resistivity measured at room temperature [18]. Absence of interatomic plane coupling provides high thermal conductivity. Graphene with defects exhibits lower thermal conductivity. Average thermal conductivity of high-quality exfoliated graphene is 3000–4000 W/m K and the thermal conductivity of graphene prepared via CVD method is 2500 W/m K [19]. Due to its excellent thermal property, graphene is being used as a temperature sensor, a thermoelectric sensor and a thermal biosensor in energy management systems [20,21]. The graphene has been synthesized using chemical vapor deposition of hydrocarbon on transition metal surfaces [22–25], thermal decomposition of silicon carbide wafer under ultrahigh vacuum [26,27], and chemical and thermal reduction of graphene oxide [28,29]. Among the methods listed above, reduction of graphene oxide is the most economical method [30]. Thus, for electrochemical analysis, graphene has been prepared using this method. In chemical vapor deposition method, there may be impurities of transition metals (Ni or Cu) but the reduction method provides graphene with high purity. Furthermore, this method provides an effective way of studying electrocatalytic effects.

Graphene oxide is a single layer of graphite oxide and is generally produced by the chemical treatment of graphite through oxidation [31]. Graphene oxide comprises various functional groups containing oxygen (see Figure 2). These functional groups are mostly hydroxyl and epoxide groups in the basal planes and consist of trace amount of carbonyl, carboxyl, phenol, lactone and quinone groups at the edges of the sheet [32]. The wide range of these functional groups at the edges and the basal planes of graphene oxide make it functionalized and exfoliated to yield well dispersed solutions of separate graphene oxide sheets in polar and non-polar solutions and therefore it has a wide range of applications in nanocomposites [33], photocatalysis [34], battery [35], capacitors [36] and sensors [37].

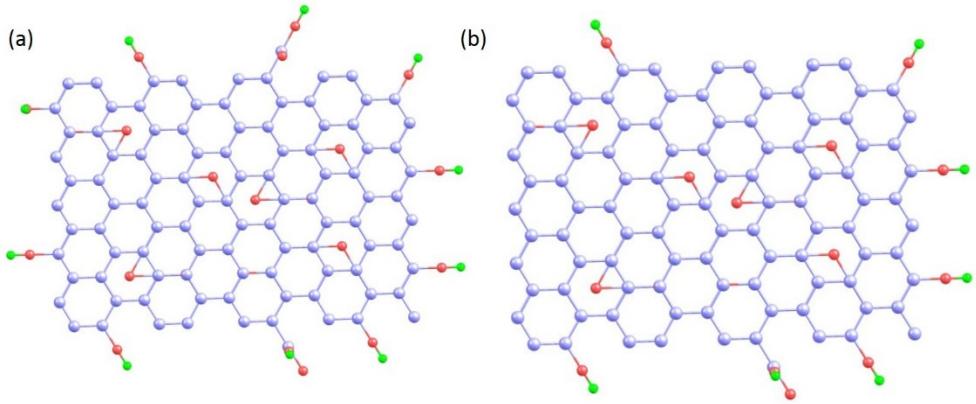

Figure 2. Structures of (**a**) graphene oxide and (**b**) reduced graphene oxide [light purple-carbon, red-oxygen and green-hydrogen].

2. Synthesis

Geim and Novoselov carried out groundbreaking experiments on the two-dimensional graphene using scotch tape method in 2004 [38]. There are bottom-up and top- down approaches available for the synthesis of graphene (see Figure 3). For example, mechanical cleavage is the process where graphite is broken down into graphene (top-down) and on the other hand, in chemical vapor deposition method, graphene is developed in silicon carbide (bottom-up) [39].

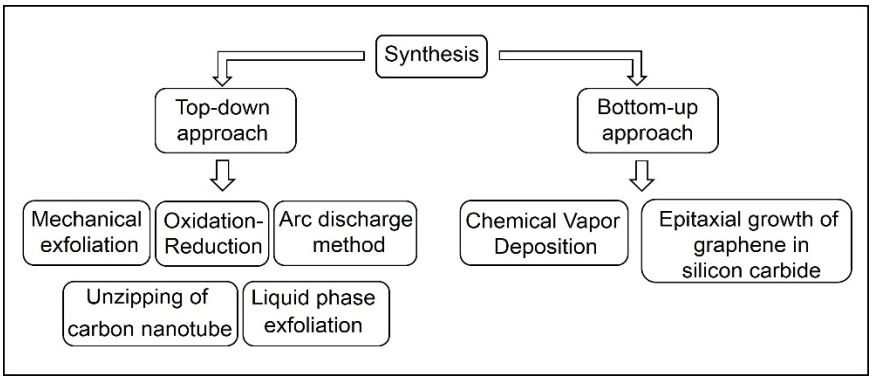

Figure 3. Schematic diagram showing synthesis methods [40].

2.1. Mechanical Exfoilation

As previously mentioned, the graphene sheets are held together by weak van der Waals forces (see Figure 4). If these forces are broken, high purity graphene can be obtained. In mechanical exfoliation method, mechanical energy is used to destroy these weak bonds and separate the individual sheets. Exfoliation is generally a peeling process repeatedly carried out in graphite to obtain layers of graphene. This method was first developed by Geim and Novoselov using highly oriented pyrolytic graphite (HOPG) as a precursor [17]. In this process HOPG sheet of thickness 1 mm is used to dry etching by oxygen plasma to create many 5 μm deep mesas (an isolated flat-topped surface). Then these were used to photoresist and baked to stick on the mesas. Thereafter, scotch tape was used to peel off the graphene layers from graphite. These thin flakes were then released to the acetone and transferred on to a Si substrate. Thus, pure graphene flakes are produced on a Si substrate. The disadvantage of this method is that large industrial production cannot be scaled.

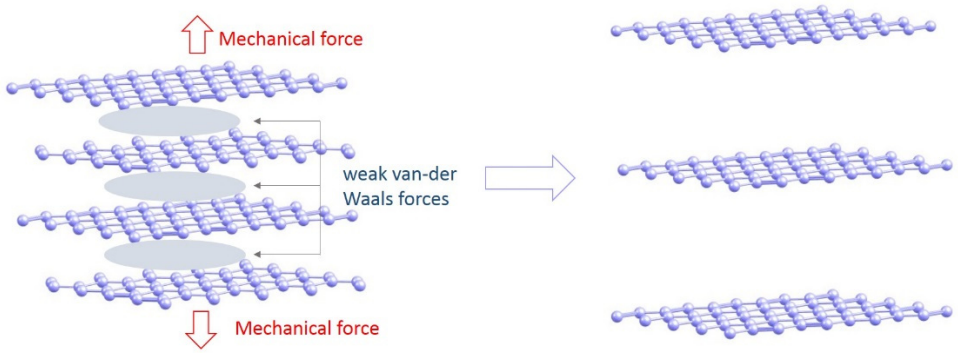

Figure 4. Mechanical exfoliation process in graphite.

2.2. Liquid Phase Exfoliation

Liquid phase exfoliation (LPE) is one of the most commonly used method for the synthesis of graphene and was first reported in 2008 [41]. In this top-down method, a stable dispersion of single layer or few-layer of graphene can be obtained through exfoliation of graphite. LPE includes main steps such as dispersion of graphite in a suitable solvent, exfoliation and the purification of the final products [42]. This method of exfoliation involves separation of graphene layers by overcoming the van der Waals forces. Therefore, the selection of solvent plays a major role. The properties such as surface energy, Hildebrand solubility, Hansen solubility parameters and surface tension have been considered for the selection of the solvent [43,44]. Researchers found that solutions with surface tension (for liquid) within 40–50 mJ/m^2 or the surface energies (for solid) within 70–80 mJ/m^2 are found to be good for the graphene production [44]. Aside for the solvent, the sonification is also an important factor to be considered during this synthesis method. Even though LPE method is an effective method for the graphene production several studies point out that sonification could affect the edges and basal planes [45]. This can be rectified by optimizing the sonification time, temperature and the sonication intensity [44]. One of the major disadvantages of this method is the yield which is not sufficient for industrial applications at macroscopic scale. Other disadvantages include solvents being expensive, toxic and the reduction of the size of the nanosheets. Future studies should be carried to improve the efficiency and the economic feasibility of this method.

2.3. Unzipping of Carbon Nanotube

This process involves cutting of the cylindrical carbon nanotubes (CNT) in axial or longitudinal direction into a flat graphene sheet with single, bi or few layers graphene. Single walled carbon nanotubes (SWCNT) or multiwalled carbon nanotubes (MWCNT) can be used as a starting material. There are several methods which have been widely investigated to unzip CNT such as plasma etching [46], chemical unzipping [47], intercalation and exfoliation [48] and metal catalyzed cutting [49]. Longitudinal unzipping of CNT leads to the formation of nanoribbons.

In chemical unzipping, CNTs were cut longitudinally by the treatment of H_2SO_4 followed by oxidation using $KMnO_4$. Then oxidized graphene will be reduced chemically using NH_4OH and hydrazine monohydrate ($N_2H_4{\cdot}H_2O$) solution [47]. This method is considered as a low significant method because during oxidation the precursor is damaged and graphene becomes electronically inferior due to the presence oxygen defect sites [47,50]. Yield of graphene was improved when intercalation of MWCNT was carried out in oxalic acid (chemical medium) prior to the chemical unzipping. The improvement in the yield was due to the appropriate size of oxalic acid (0.34 nm) which intercalates comfortably between the interlayers of the MWCNT [51]. In plasma etching, polymer film such as poly-methyl methacrylate is being used. In this method, CNT is embedded into the film and then this mixture of film and CNT are separated out in KOH solution. Thereafter CNT is exposed in argon-based plasma. Here the longitudinal C-C bond of CNT is broken down to produce graphene with smooth edges [46]. Intercalation and exfoliation is another

method of unzipping CNT. Here lithium and ammonia are allowed to react with CNT. In this treatment, a strong stress is exerted between the layers of CNT resulting in the separation of the graphene layers [48]. Researchers considered other metal nanoparticles such as nickel, cobalt and copper and found that C-C and H-H bonds in MWCNT were dissociated by these nanoparticles [52]. The above-mentioned methods use chemicals which are hazardous and expensive. Unzipping of MWCNT can be achieved by using electric field from tungsten electrode [53]. This method provides defect free and high pure graphene nanoribbons. Therefore, electric field method is more preferable due to feasibility, environmentally friendliness and accuracy.

2.4. Arc Discharge Method

In Arc discharge method, anode and cathode are submerged in a gas or liquid medium of a reaction chamber. During the passage of electricity, the medium is dissociated to produce a high temperature plasma (3727–5725 °C) and this will be sufficient to sublime the precursor [54]. This method is considered to be expensive due to the usage of vacuum. Therefore, the use of air instead of H_2/He medium is preferred to reduce the cost of production of graphene [55]. Li et al. demonstrated a method in which petroleum asphalt is used as a precursor in a water arc discharge system [55]. The use of asphalt which is a carbon rich source and water medium makes this method a cost effective. These improvements in arc discharge method could produce graphene at an affordable price.

2.5. Chemical Vapor Deposition (CVD)

CVD is one of the most promising method for the synthesis of graphene cost effectively and can produce large area of graphene. In this CVD approach, hydrocarbon gaseous species are injected into the reactor and travel through a hot zone where these molecules degrade to form carbon radicals and deposit on the metal surface as single / few layer graphene (see Figure 5). During this process metal surface acts as a catalyst and also influences the deposition mechanism of graphene which plays a key role in the preparation of pure graphene [56]. Researchers have used metals such as Ru, Ir, Pt, Co, Pd and Re. The nickel (Ni) and copper (Cu) are low cost, have better control of layers of graphene and are easier to transfer graphene. Thus, they are widely used as substrates in CVD [56]. Using cold-wall and hot-wall reaction chambers, the CVD growth of graphene has been carried out [57]. In this technique, the growth of graphene is fast, high quality and takes low power consumption. Furthermore, there is an enhancement in charge carrier mobility.

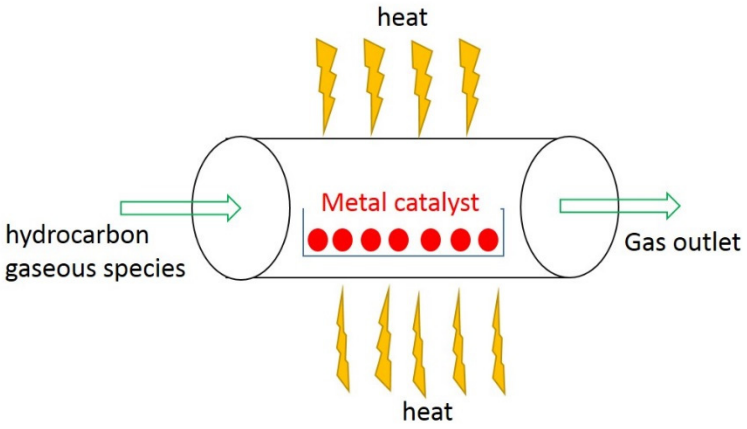

Figure 5. Schematic diagram showing CVD approach.

2.5.1. Chemical Vapor Deposition of Graphene on Nickel

In this synthetic method, Ni films are first annealed at 900 to 1000 °C under Ar/H_2 environment for 20 min to increase the grain size of Ni. Thereafter film is exposed to CH_4/H_2 mixture. Here the methane is degraded to form carbon atoms and dissolves into the film resulting a solid solution. As the last step, these samples are cooled in argon gas.

Ni is highly soluble in carbon at elevated temperature and it reduces with the decreasing temperature [56]. The formation of thickness was dependent on the rate of cooling [58].

2.5.2. Chemical Vapor Synthesis of Graphene on Copper

In this method, Cu foil of thickness 25 μm was heated at 1000 °C in hydrogen atmosphere followed by the introduction of H_2/CH_4 mixture to initiate the formation of graphene. Then the temperature was reduced to room temperature [56]. One of the demerits of this method is that Cu has the very low solubility of carbon even at high concentration of hydrocarbon or longer growth time [56].

2.6. Epitaxial Growth of Graphene in Silicon Carbide (SiC)

Epitaxial growth can be made under vacuum or at atmospheric conditions. Different types of SiC such as single crystal SiC wafers, polycrystalline SiC and SiC thin films are used in this method. SiC is heated to 1200–1600 °C in ultra-high vacuum which sublimates silicon (melting point of Si = 1100 °C) leaving carbon atoms in the reaction vessel. Later these carbon atoms aggregate to form graphene [59]. This method produced 1 to 3 layers of graphene and the number of layers dependent on the decomposition temperature [14]. This synthetic technique is capable of producing wafer scale layers of graphene and therefore its potential interest is high in the semiconductor industry [14]. As a development of this method, graphene was synthesized from Ni coated SiC substrate at a lower temperature of 750 °C [60]. This method consists of technical problems such as high cost of SiC substrates (single-crystal SiC) and high temperature. These issues should be properly addressed to extend the practical and economic feasibility.

2.7. Oxidation-Reduction

This is one of the widely used methods for the synthesis of graphene from graphite. There are four major routes available for the conversion of graphite to form graphene oxide such as Brodie [61], Staudenmaier [62], Hofmann [63] and Hummers [31] method. All these methods are almost similar to each other except the use of different chemicals and improved steps over the years. All these methods require temperature below 100 °C to maintain low production cost. One of the demerits of these methods is the release of toxic gases such as nitrogen dioxide (NO_2) and dinitrogen tetroxide (N_2O_4) [64,65]. Nowadays the Hummers method is being widely used as this method is fast and safe (see Figure 6). Recent modified version of hummers' method has eliminated the use of sodium nitrate ($NaNO_3$) which reduces the production cost [66]. The oxidation of graphene increases the inter layer spacing of graphite layers from 0.335 to 0.625 nm. This is because of the incorporation of intercalation compounds [67]. This confirms the reduction of van der Waals forces between the inter layers. Therefore, exfoliation by sonication using a suitable solvent can produce single or bilayer or few layer graphene oxide (GO) [67]. Graphene does not contain any functional groups and it is therefore insoluble in water and organic solvents. On the other hand, GO is hydrophilic due to the presence of functional groups containing oxygen that can be dispersed in different solutions such as water, tetrahydrofuran (THF) and ethylene glycol [68]. Reduction methods are used for the restoration of honeycomb lattice from disrupted sp^2 bonding of GO. Mainly chemical, thermal and electrochemical processes are used for the reduction of GO eliminating the oxygen functional groups such as carbonyl, carboxylic and hydroxyl.

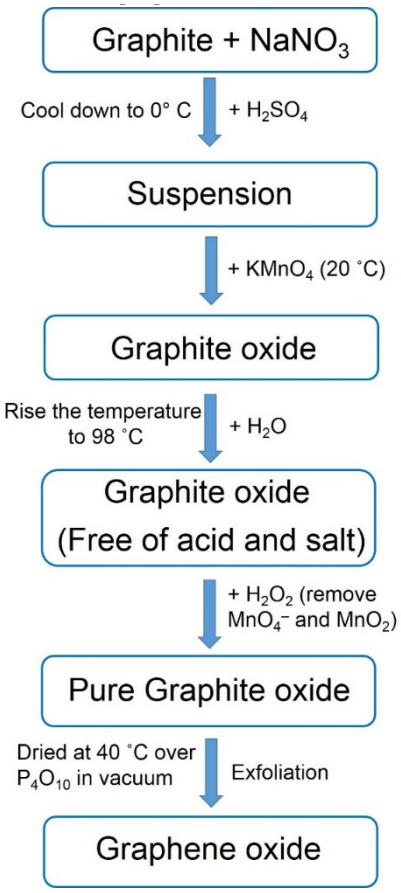

Figure 6. Schematic diagram showing Hummers method [31].

In a chemical reduction of GO, hydrazine (N_2H_4) is commonly used. However, it is a toxic chemical and relatively expensive for the production. Therefore, several reducing agents such as borohydride, aluminum hydride, plant extract, amino acids and microorganism have been widely used [69]. Due to the safety, environmental concerns and synthesis time, thermal reduction [70] and hydrothermal reduction [71] have been investigated by the scientists. Thermal reduction method has demerits such as high temperature, high cost and release of greenhouse gas CO_2 meanwhile hydrothermal reduction requires low temperature there by lower energy consumption [72]. Electrochemical reduction has gained considerable interest owing to its rapid reduction, environmentally benign (fewer toxic reductants) and cost effectiveness [40].

3. Applications

3.1. Lithium Ion Batteries

Rapid decrease of fossil fuels and the environmental pollution necessitated the invention of new energy sources. Lithium ion battery was first introduced in 1999. In 2019, John B. Goodenough, M. Stanley Whittingham and Akira Yoshino were awarded noble prize in chemistry for the invention of Lithium ion batteries (LIBs). Owing to the long cycle and high energy density, LIBs are considered as important energy storage devices. Graphene has been widely investigated for the anode material for LIBs because of its high flexibility, stability and high surface to volume ratio. The speed of Li ion movement determines the power capability of battery [73]. Application of the graphene with transition metal oxides improves the discharge rate and electrochemical stability.

Graphitic carbon has been used as an anode material for LIBs. It possess high crystallinity. Layer arrangement leads to the formation of LiC_6 which is the highest intercalation state of the battery [74]. Zhao et al. reported anodic material prepared by electrochemical exfoliation and it exhibited a capacity of 356 mA h g^{-1} at 1 A g^{-1} with 100% capacity re-

tention after more than 6500 cycles [75]. Ji et al. [76] reported a novel 3D graphene powder synthesized via thermal CVD. Incorporation of this powder in graphite electrode consisted a capacity of 542.8 mA h after 400 cycles and 427.2 mA h after 1000 cycles [76]. Density functional theory calculations reported by Oladipo et al. revealed that the graphene loaded with polypyrroles exhibited a small band gap of 0.39 eV and strong absorbing power [77].

Nanoparticles were allowed to intercalate with graphene to improve the performance of the batteries. Graphene intercalated with Co_3O_4 nanoparticles was analyzed as an anode material for high performance LIBs. Here the nanoparticles were intercalated between sheets to maintain the separation of sheets [73]. This intercalation improved cyclic performance and resulted in high reversible capacity. This combination was found to have specific capacity of 1100 mA h g^{-1} with current density of 74 mA h g^{-1}. After 130 cycles the discharge capacity was observed at 1000 mA h g^{-1} [78]. In another study, SnO_2-graphene intercalation was investigated and charge capacity of 860 mA h g^{-1} with current density of 50 mA g^{-1} was observed. This attainment was due to the nanocrystalline property of SnO_2-graphene. Reversible capacity was found at 810 mA h g^{-1} and 70 % of the reversible capacity was remained after 30 cycles at 570 mA h g^{-1} [79]. Rutile TiO_2-graphene composite have the specific capacity of 87 mA h g^{-1} and anatase TiO_2-graphene have the high current density of 96 mA h g^{-1} [80]. Silicon-boron nitride nanocomposite displayed a reversible capacitance of 785 mA g^{-1} at 450 mA g^{-1} at the end of 800 cycles. The incorporation provides a large Li-ion storage and shorter Li-Li separation [81].

Addition of heteroatoms such as B and N into the graphene frameworks improved the surface wettability due to the presence of more hydrophilic sites and improved reactions between electrolyte and electrode [82]. N-doped graphene was studied for the reversible discharge capacity and it was found that nitrogen atoms improved the Li ion intercalation [83]. In a recent study, N-doped graphene nanosheets were synthesized in ammonia (NH_3) environment by heat treatment of graphene oxide. Reversible capacity of around 250 mA h g^{-1} at 2.1 mA g^{-1} current density and capacity of 900 mA h g^{-1} at 4.2 mA g^{-1} were obtained [84]. Yang et al. reported the fabrication of N-doped porous graphene hybrid nanosheets with induced growth of zeolitic imidazolate framework on graphene [85]. This framework on graphene increases the specific area and the electron transfer within graphene network [85]. Hetero atomic defect increased the distance between sheets and electrolyte wettability enhanced the thermal stability and the electrical conductivity of doped graphene [86]. Graphene has been studied as mostly as anode material instead of cathode material because of its low electrical conductivity, slower electron and Li ion transport and low specific capacity and the agglomeration of the particles while applied as the cathode material [87]. Among the studies reported above, graphene intercalated with Co_3O_4 nanoparticles has high specific capacity and current density. Here the nanoparticles intercalate between graphene sheets and flexibility of graphene increased it performance. There is a strong interaction between graphene and Co_3O_4 preventing volume expansion/contraction and aggregation of nanoparticles during the battery performance. Yusuf et al. [73] reported that this composite effectively shows high surface area, good conductivity, and mechanical flexibility. Thus, this Co_3O_4—graphene composite exhibits a better performance.

3.2. Supercapacitors

Supercapacitors are energy storage devices with good cyclability, high power and fast charge-discharge process [72]. Surface area of the materials used for the fabrication of supercapacitors determines the performance. Several materials have been widely investigated to improve the performance. Among those, graphene and graphene-based composites have received attention owing to their high surface area, distinctive mechanical and electrical properties. Agglomeration of graphene has been mentioned as a major drawback in the performance of supercapacitors. This can be overcome by the incorporation of metal oxide nanoparticles with graphene [72].

Metal oxides such as RuO_2, NiO_2, MnO_2, ZnO and SnO_2 have been investigated to enhance the performance of supercapacitors. Deposition of RuO_2 on the surface of graphene prevents agglomeration and improves electron transfer. High conductivity of RuO_2 nanoparticles and separated graphene sheets provide combined advantage and improved performance with the energy density of 20.1 $Whkg^{-1}$ and an excellent electrochemical stability of 97.9% after 1000 cycles [88]. $Ni(OH)_2$-graphene hydrogel was found to have specific capacitance of ~1212 F g^{-1} at the discharge rate of 2 A g^{-1} [89]. Supercapacitor fabricated with graphene-carbon nanotube (CNT) hybrid attained the highest energy density among the all carbon-based supercapacitors and was found to work at 4V and possess energy density of 460 $Whkg^{-1}$ [90]. This is due to the large surface area and the covalent interaction between graphene and carbon nanotubes. Porous Nickel-graphene-CNT exhibits high diffusion conductivity which is due to the aligned interfacial contact and volume of the 3D nanomaterial [91]. Three-dimensional flower shaped $Li_4Ti_5O_{12}$-graphene nanostructure exhibits a high specific capacitance of 706.52 F g^{-1} with discharge rate of 1 A g^{-1} and pine needles-based carbon nanostructure possess specific capacitance of 314.50 F g^{-1} at the discharge rate of 1 A g^{-1}. Supercapacitor with $Li_4Ti_5O_{12}$-graphene nanostructure as a positive electrode and pine needles-based carbon nanostructure as a negative electrode provides an energy density of 35.06 $Whkg^{-1}$ with power density of 800.08 W kg^{-1} and exhibit cyclic stability of 90.18% after 2000 cycles, respectively [92]. Graphene-MoS_2 composite prepared by Wang et al. [93] exhibits higher specific capacitance when compared with that of graphene. This combination gives the interconnection and interpenetration between nanomaterials which reduced restacking and aggregation. This composite exhibits a capacitance of 58.5 mF/cm^{-2} and showed quick current response to voltage reversal [93].

Chen et al. [94] have reported novel network structure of nitrogen doped porous graphene and this network possessed good conductivity and quick electron transfer. This network has high gravimetric capacitance and volumetric capacitance compared to that of graphene. This supercapacitor exhibits energy density up to 27.6 Wh Kg^{-1} at 600 W kg^{-1} [94]. Graphene based aerogels have been an excellent candidate as electrode materials because of their ultralow density, mechanical stability and flexibility [95,96]. Doping the aerogels with N and S increased the performance of the supercapacitor. Zhang et al. [97] reported the synthesis of N, S co-doped graphene aerogels using 2,5-Dimercapto-1,3,4-thiazole as a precursor. This exhibited a capacitance of 321 F g^{-1} at a current of 1 A g^{-1} which is approximately twice the value of pure graphene aerogel. Here the S and N atoms improved the performance of supercapacitor through synergistic effect [97]. It is generally expected that high specific surface area provides high specific capacitance of carbon-based electrodes. Graphene nanoflakes reported by Arkhipova et al. [98] had specific surface area range of 1720 to 660 m^2 g^{-1} depending on the synthesis time. The highest capacitance of 112 Fg^{-1} was observed for the graphene nanoflakes synthesized in the shortest synthesis time [98]. In supercapacitors, the application of nanoparticles with graphene improves the performance by preventing the agglomeration. Nitrogen doped graphene possess high performance than the graphene made of nanoparticles. This is due to the improvement in the electron transfer via nitrogen doping.

3.3. Electrochemical Sensors

Electrochemical sensing is one of the most important application of graphene. The adsorption of molecules on the surface of graphene influences its electrical conductivity [10]. Carrier concentration of the graphene is dependent on the type of dopant (donor or acceptor) adsorbed on the surface. There are many properties of graphene which increase its efficiency of detecting molecules. Since graphene is a 2D material, whole surface can be exposed to the analyte [99]. Graphene has high conductivity and low noise of distortion. Thus a small change in the concentration can alter electrical conductivity [98]. It consists of very low crystal defects [17,100] which ensure the low noise of distortion due to the thermal switching [101]. Schedin et al. [99] first reported the sensing of graphene in 2007. In this

report sensing of gas molecules such as NO_2, NH_3, H_2O and CO is discussed. Re-usage of graphene sensors after the vacuum annealing at temperature of 150 °C or under UV radiation is possible for a short time [99].

Fowler et al. [102] reported the sensing of NO_2, NH_3 and dinitro toluene (DNT, used in explosives) by graphene [102]. Sensing of NO_2 was occurred by the withdrawal of electron from the graphene (hole induced conduction) and in NH_3, electron was donated to the graphene from the gas molecules (electron induced conduction). This explains that the sensing occurs due to the transfer of charge (donation or acceptance) at the surface of graphene [102]. Sundaram et al. [103] have reported the sensing of H_2 on the modified graphene by the deposition of Pd nanoparticles (Nps) and Pd showed high affinity towards H_2. Here the resistance of the bare and Pd-modified graphene sheets has almost the same resistance maximum in the gate dependence curve. During the adsorption of H_2, resistance maximum is strongly shifted to the negative gate voltages. This shift is due to the dissolution and partial dissociation of hydrogen at Pd nanoparticles. The particle's work function decreases as the electrons are transferred from Pd to the graphene sheet. [82]. Gupta et al. [104] reported the ascorbic acid sensor by graphene nanosheets functionalized with polyaniline nanostructures and metal nanoparticles (Au Nps, Ag Nps). Here the nanoparticles are sandwiched between layers of graphene to ensure the good electron transfer. This can be further improved by changing the morphology, size, and the density of particles. Graphene sensor was found to have ultrasensitive up to lower concentration of 1×10^{-12} M and sensor with Au nanoparticles had a low signal-to-noise ratio. [104].

Shan et al. [105] have reported the sensing of glucose using graphene functionalized with glucose enzyme oxidase (GOD). Biosensor was comprised of graphene-polyethyleneimine-functionalized nanocomposite for the detection of glucose. Flavin adenine dinucleotide (FAD) is deeply embedded in a protective protein shell, which makes the direct electron communication difficult with electrodes. As the graphene has the high specific area and extraordinary electron transport, direct electron transfer between GOD and electrode substrate is promoted. Sensor was based on the electron transfer from GOD demonstrating the potential application of graphene in glucose detection. A linear response was recorded between 2 mM to 14 mM in their study [105]. Kang et al. [106] have constructed a glucose sensor employing chitosan. They have sonicated suspension containing graphene and chitosan for 1 h and a stable dark suspension was formed as a result. This results in the formation of C-OH and -COOH functional groups which let the graphene more hydrophilic. Chitosan disperses the graphene and immobilizes the enzyme molecules and this sensor showed a sensitivity of 37.93 $\mu A\ mM^{-1}\ cm^{-2}$ for the concentration ranging between 0.08 mM and 12 mM possessing a long-term stability [106]. As the diabetic glucose concentration is above 7.0 mM and this sensor can be used for the determination of human blood sugar level. The linear range of this sensor is wider than that reported by Liu et al. [107], 0 to 7.8 mM (GOD on MWCNTs-chitosan matrix), Liu and Ju, et al. [108] 0.08 to 0.28 mM (GOD on colloidal gold modified carbon paste electrode) and Huang et al. [109] 0.5 to 11.1 mM (GOD at a Cds nanoparticles modified electrode). Wu et al. [110] reported sensor GOD-graphene-PtNps-chitosan which has a detection of 0.6 µM glucose. Performance of this sensor was increased through intercalation of nanoparticles with graphene in order to increase the larger surface area and electrical conductivity. Here the interfering signals from the ascorbic acid and uric acid are negligible compared with the response to glucose [110,111].

Graphene based DNA electrochemical sensors provide a high sensitivity, high selectivity and low cost for the detection of DNA sequences and genes which are mutated and provide a simple and promising diagnosis of patients [112,113]. Sensor is based on the change in conductivity as the DNA molecules are physiosorbed on the graphene surface resulting in the change in the conductivity [114,115]. Zhou et al. [116] have reported DNA electrochemical sensor based on graphene obtained from chemical reduction of graphene oxide. The sensor detects four different current signals of nucleotide bases in DNA (guanine, adenine, cytosine and thymine) [11]. These devices can be separated into two namely, back-gated and liquid-gated [117]. Compared with that of the back-gated sensors, liquid-

gated sensors are used widely for the detection of the DNA due to the sensitivity of 0.01 nM and ability to detect single mismatches [118]. This sensor has two electrode sources and a drain which connected by graphene sheet. A drop of buffer with DNA sample is loaded on the graphene surface then the gate voltage is measured so that DNA templates can be identified [119].

Electrochemical sensors based on graphene have been developed for the detection of the heavy metal ions. Li et al. [119,120] have identified a sensor based on Nafion-graphene composite film for the detection of Pb^{2+} and Cd^{2+}. The detection limits of 0.02 μL^{-1} were observed for both heavy metal ions. The linear range is 0.5 μL^{-1} to 50 μL^{-1} and 1.5 μL^{-1} to 30 μL^{-1} for Pb^{2+} and Cd^{2+}, respectively. The sensitivity was found to be higher than Nafion -bismuth electrode [121] and Nafion-CNT coated bismuth film electrode [122]. The enhanced performance is due to the unique properties of graphene such as capacity to adsorb metal ions [119,120].

3.4. Transparent Electrodes

Indium titanium oxide (ITO) and fluorine doped tin oxide (FTO) are commonly used as transparent coating for liquid crystal displays, solar cells and touch panels [123]. Due to the brittle nature and expensiveness of indium, graphene is being studied for the application in the transparent electrodes. The unique chemical, physical and mechanical stability makes graphene perfect material as a transparent electrode for solar cell and displays. Large surface area, inertness towards water and oxygen, high hole transparent mobility make graphene as an ideal material for photovoltaics [14].

Kim et al. [124] reported the growth of graphene films on a 300 nm thick nickel layer and the transmittance was reported to be 80%. Graphene layer is grown on the nickel surface by CVD and then the Nickel can be etched away using $FeCl_3$ leaving the graphene film alone. The reduction in the thickness of the nickel layer and growth time increases the transmittance to 93%. It was mentioned that further reduction of graphene layer thickness by ultraviolet etching increased the sheet resistance. In order to reduce the contact resistance, indium electrodes were deposited on the corner of the square. The minimum sheet resistance is around 280 Ω per square, which is around 30 times smaller than the lowest sheet resistance measured on assembled films [124]. Wang et al. [125] prepared a transparent graphene electrode for dye sensitized solar cells (DSSC) from exfoliated graphene oxide followed by thermal reduction. It was found that it has 70% of transparency over 1000 to 3000 nm and a good conductivity of 550 S/cm. It possesses short circuit photocurrent density of 1.01 mA cm^{-2}, open circuit of 0.7 V and overall power conversion efficiency of 0.26%. Low conversion efficiency was due to the low quality of graphene film [125]. Hong et al. [126] mentioned that composites of graphene with poly (3.4-ethylenedioxythiophene) had the transmittance of more than 80% and the energy conversion efficiency of 4.5%. The thickness of the synthesized film was around 60 nm. When the graphene weight percentage in the composite increased from 0 to 1 %, it was observed that the energy conversion was increased from 2.3 % to 4.5 %. This weight percentage was optimum and further increase of the weight percentage of graphene resulted in the reduction of the energy conversion efficiency [126]. Cu was chosen as a transparent electrode due to its low cost and high electrical conductivity. Thickness of the metal plays a crucial role in the performance because higher thickness gives improved resistance but reduces the transmittance. Kang et al. [127] reported the performance of Cu with different thickness (1, 3, 5, and 7 nm) incorporated with graphene. When the thickness of Cu is higher than 5 nm, the intensity of light entering the electrode is reduced. Cu with thickness of 3 nm exhibits a maximum current density of 12.64 mA/cm^2 [127]. Huang et al [128] reported a sandwich structure made of graphene and silver nanowire where silver nanowire is inserted between two layers of graphene. The stretchable properties of single layer graphene (SLG), double layer graphene (DLG) and sandwiched type structure was analyzed and it was observed that the resistance of the SLG was unmeasurable after 10 cycles, DLG have similar results after 40 cycles but the sand witched type gradually

increased to 4 after 20 cycles. Thereafter conductivity structure stabilized up to 100 cycles. This sandwiched type structure exhibits an excellent stretching ability. Under tensile strain cracks and holes were formed in SLG (15.14 %) and DLG (10.28 %) but sandwiched type electrode only experienced fewer cracks and holes (6.4%). This result indicates that the Ag wire suppress the crack formation. This structure effectively reduces the oxidation of the silver wire and withhold the initial resistance of the electrode. Furthermore, it possessed low sheet resistance, high light transmittance (greater than 90 %) and long-term stability when compared to that of SLG and DLG [128].

3.5. Environmental Applications

With the start of industrial revolution in the mid-18th century, many advanced industries were developed with the use of steam, coal and fossil fuels. During this period, environmental pollution started to increase rapidly. Many mining industries released metal ions to the environment. Advancement of motor vehicles and the use of fossil fuels increased the greenhouse gases and other hazardous gases to the environment. Graphene and its derivatives play a crucial role in removing these pollutants from the environment.

3.5.1. Adsorption of Metal Ions

Metal ion pollutants enter into water bodies due to mining and industrial wastes. Generally, activated carbon has been used for the adsorption of metal ion pollutants, however, its production cost and regeneration restrict its applications. Owing to the high surface area, tunable surface chemistry, scalable production and non-corrosive property provide a path for the graphene-based materials for the application in metal ion adsorption [129,130]. Nanoparticles such as iron or iron oxide have been incorporated with the graphene (magnetic graphene nanocomposite) for the adsorption. Here the iron oxide is used to remove the chromium (VI). The graphene and magnetic graphene nanocomposite were compared for the Cr (VI) removal ability. The pure graphene exhibited lower removal efficiency of only 44.6 % (even high concentration of 3 g L^{-1}) while the magnetic graphene nanocomposite showed a higher removal of efficiency of 52.6 % (at lower concentration 0.25 g L^{-1}). The removal efficiency is further improved to 100 % when the 10% nanoparticle loaded with magnetic graphene nanocomposite. This composite completely removes Cr (VI) within 5 min (using 3 g L^{-1}). pH plays an important role for the adsorption of Cr (VI) and adsorption efficiency was higher at lower pH range (pH 1–3). [131,132]. Here the graphene is used as a physical support for iron oxide nanoparticle which improves the surface area and increases the number of binding sites for the metal ions [132]. Magnetically active iron oxide can be efficiently removed from solution using its magnetic properties [133].

3.5.2. Adsorption of Gases

Gosh et al. [134] have studied the adsorption of CO_2 and H_2 on the graphene surface and found that maximum adsorption of 37.93 % takes place by a single layer of graphene. Highest adsorption of H_2 was adsorbed around 3.1 weight % and the CO_2 adsorption was around 21–34 weight % [134]. Density functional theory study on the CO_2 adsorption on defective graphene sheets indicates that CO_2 is adsorbed exothermally on the vacancy defects in the graphene sheets. The energy of physisorption of CO_2 on the monovacancy site is around 210 m eV and the chemisorption energy is around 1.72 eV. Further studies revealed that the defective graphene showed four times higher adsorption than defect free graphene and CO_2 molecules could form C-O bond with the carbon atoms of graphene [135]. Liu et al. [136] have studied the influence of the oxygen functional group on the adsorption using CO_2-CH_4, CO_2-N_2, CO_2-H_2O mixtures. The results indicated that the CO_2 which have the oxygen functional group is preferentially adsorbed over CH_4 and N_2. CO_2 is preferentially adsorbed on the functionalized graphene surface with an induced polarity due to the strong quadrupolar moment of CO_2 compared to the species of N_2 and CH_4 where the quadrupole is week. In the CO_2-H_2O mixture, H_2O is adsorbed relatively

higher. This study revealed that the surface of the graphene can be tuned for the selective adsorption of gaseous molecules [136].

3.5.3. Graphene Based Photocatalyst

Owing to the low cost and oxidizing ability, TiO_2 is generally used as a semiconductor forming graphene based photocatalyst for the degradation of the organic and biological contaminants. Reduced graphene oxides with 10% of Titanium nanotubes (TNT) showed the photocatalytic degradation of three times higher than the free TNT. TNTs were preferred due to their larger surface area when compared with that of the spherical nanoparticles [137]. As the organic dyes are aromatic, their adsorption on the graphene surface is enhanced by the π-π stacking interaction between sp^2 orbitals of the both systems [138]. Due to the combination of the graphene and photocatalyst, the band gap of the photocatalyst is reduced thus increasing the efficiency of the degradation [138,139]. Graphene improves the electron-hole recombination through the sp^2 hybridized network. Here the graphene acts as an electron acceptor and gives a conductive platform to transport electrons which involves in the oxidation and reduction reaction during degradation [138].

4. Conclusions

Graphene is a two-dimensional carbon network with a considerable research interest. Owing to its unique chemical and physical properties graphene has been investigated and used in many applications such as electronics, energy storing batteries, supercapacitors, solar cells and photocatalysts. Several synthetic methods have been applied to produce graphene such as mechanical exfoliation, liquid phase exfoliation, unzipping of carbon nanotubes, chemical vapor deposition and oxidation and reduction. Among these methods, chemical vapor deposition is the most promising method as this method is cost effective and can produce a large amount of graphene. N-doped graphene nanosheets and nanoparticles incorporated graphene have been investigated to improve the performance of the lithium ion batteries. The incorporation of nitrogen with graphene increases specific area and electron transfer within the network of graphene. Metal oxide nanoparticles such as RuO_2, NiO_2, MnO_2, Co_3O_4, ZnO and SnO_2 and CNT-graphene have been incorporated with graphene to boost the performance of the super capacitors. Among these Co_3O_4 nanoparticles exhibit the best performance. Both graphene and Co_3O_4 have strong interaction and this helps to prevents volume expansion/contraction and the aggregation of nanoparticles. Several electrochemical sensors such as gas sensors, biomolecular sensors and heavy metal ion sensors have been under research and in application as well. Sensors have been developed by the incorporation of metal nanoparticle and used to track NO_2, NH_3, DNT, CO, glucose level, DNA sequences, and metal ions (Pb^{2+}, Cd^{2+}). Biosensors have been developed with chitosan protein. Chitosan protein provides functional groups to make the sensors hydrophilic. Nanoparticles play an important role in these sensors by increasing the performance. Theses biosensors have been utilized for the detection of blood glucose level. Graphene has been studied for the transparent electrode in DSSC and several studies have been undergoing to improve the light conversion efficiencies. Graphene has been developed on Ni (1.01 mA cm^{-2}) and Cu to use as transparent electrodes. Performance of the transparent electrode was depended on the thickness of the metal and the weight percentage of the graphene. As Cu is a low cost and high electrical conductivity material, has an excellent performance of 12.64 mA/cm^2, when compared with the Ni. Unique chemical property of the graphene paved the way for the environmental applications such as adsorption of heavy metals, organic contaminants, gases and applications, where graphene functions as photocatalyst for the degradation of the organic pollutants. Compared to the adsorption of the gases CO_2, H_2O, CH_4, and N_2, CO_2 was preferentially adsorbed by functionalized graphene. As levels of CO_2 is drastically increasing this might be a solution to reduce the levels of CO_2 and to tackle the climate change. Graphene remains as a unique material with exceptional properties that could lead to promising applications.

Author Contributions: Conceptualization, A.S., P.I. and P.A.; data curation, A.S.; writing—original draft preparation, A.S.; writing—review and editing, N.K.; All authors have read and agreed to the published version of the manuscript.

Funding: This research received no funding.

Acknowledgments: We acknowledge the Department of Chemistry, University of Jaffna for providing technical support during the preparation of the manuscript.

Conflicts of Interest: The authors declare no conflict of interest.

References

1. Fang, B.; Chang, D.; Xu, Z.; Gao, C. A Review on Graphene Fibers: Expectations, Advances, and Prospects. *Adv. Mater.* **2020**, *32*, 1902664. [CrossRef]
2. Hass, J.; De Heer, W.A.A.; Conrad, E.H. The growth and morphology of epitaxial multilayer graphene. *J. Phys. Condens. Matter* **2008**, *20*, 323202. [CrossRef]
3. Yoo, E.; Kim, J.; Hosono, E.; Zhou, H.-S.; Kudo, T.; Honma, I. Large Reversible Li Storage of Graphene Nanosheet Families for Use in Rechargeable Lithium Ion Batteries. *Nano Lett.* **2008**, *8*, 2277–2282. [CrossRef]
4. Stoller, M.D.; Park, S.; Zhu, Y.; An, J.; Ruoff, R.S. Graphene-Based Ultracapacitors. *Nano Lett.* **2008**, *8*, 3498–3502. [CrossRef] [PubMed]
5. Kou, R.; Shao, Y.; Wang, D.; Engelhard, M.H.; Kwak, J.H.; Wang, J.; Viswanathan, V.V.; Wang, C.; Lin, Y.; Wang, Y.; et al. Enhanced activity and stability of Pt catalysts on functionalized graphene sheets for electrocatalytic oxygen reduction. *Electrochem. Commun.* **2009**, *11*, 954–957. [CrossRef]
6. Wu, J.; Becerril, H.A.; Bao, Z.; Liu, Z.; Chen, Y.; Peumans, P. Organic solar cells with solution-processed graphene transparent electrodes. *Appl. Phys. Lett.* **2008**, *92*, 263302. [CrossRef]
7. Sun, S.; Gao, L.; Liu, Y. Enhanced dye-sensitized solar cell using graphene-TiO_2 photoanode prepared by heterogeneous coagulation. *Appl. Phys. Lett.* **2010**, *96*, 083113. [CrossRef]
8. Balandin, A.A.; Ghosh, S.; Bao, W.; Calizo, I.; Teweldebrhan, D.; Miao, F.; Lau, C.N. Superior Thermal Conductivity of Single-Layer Graphene. *Nano Lett.* **2008**, *8*, 902–907. [CrossRef]
9. Service, R.F. Materials science. Carbon sheets an atom thick give rise to graphene dreams. *Science* **2009**, *324*, 875–877. [PubMed]
10. Lee, C.; Wei, X.; Kysar, J.W.; Hone, J. Measurement of the Elastic Properties and Intrinsic Strength of Monolayer Graphene. *Science* **2008**, *321*, 385–388. [CrossRef]
11. Zheng, P.; Wu, N. Fluorescence and Sensing Applications of Graphene Oxide and Graphene Quantum Dots: A Review. *Chem.—Asian J.* **2017**, *12*, 2343–2353. [CrossRef] [PubMed]
12. Allen, M.J.; Tung, V.C.; Kaner, R.B. Honeycomb Carbon: A Review of Graphene. *Chem. Rev.* **2009**, *110*, 132–145. [CrossRef]
13. Enoki, T.; Endo, M.; Suzuki, M. *Graphite Intercalation Compounds and Applications*; Oxford University Press: New York, NY, USA, 2003; p. 452.
14. Choi, W.; Lahiri, I.; Seelaboyina, R.; Kang, Y.S. Synthesis of Graphene and Its Applications: A Review. *Crit. Rev. Solid State Mater. Sci.* **2010**, *35*, 52–71. [CrossRef]
15. Nimbalkar, A.; Kim, H. Opportunities and Challenges in Twisted Bilayer Graphene: A Review. *Nano-Micro Lett.* **2020**, *12*, 1–20. [CrossRef]
16. Bacon, M.; Bradley, S.J.; Nann, T. Graphene Quantum Dots. *Part. Part. Syst. Charact.* **2014**, *31*, 415–428. [CrossRef]
17. Geim, A.K.; Novoselov, K.S. The rise of graphene. *Nat. Mater.* **2007**, *6*, 183–191. [CrossRef] [PubMed]
18. Chen, J.-H.; Jang, C.; Xiao, S.; Ishigami, M.; Fuhrer, M.S. Intrinsic and extrinsic performance limits of graphene devices on SiO2. *Nat. Nanotechnol.* **2008**, *3*, 206–209. [CrossRef]
19. Balandin, A.A. Phononics of Graphene and Related Materials. *ACS Nano* **2020**, *14*, 5170–5178. [CrossRef]
20. Rhee, K.Y. Electronic and Thermal Properties of Graphene. *Nanomaterials* **2020**, *10*, 926. [CrossRef]
21. Guo, X.; Cheng, S.; Cai, W.; Zhang, Y.; Zhang, X.A. A review of carbon-based thermal interface materials: Mechanism, thermal measurements and thermal properties. *Mater. Des.* **2021**, *209*, 109936. [CrossRef]
22. Reina, A.; Jia, X.; Ho, J.; Nezich, D.; Son, H.; Bulovic, V.; Dresselhaus, M.S.; Kong, J. Large Area, Few-Layer Graphene Films on Arbitrary Substrates by Chemical Vapor Deposition. *Nano Lett.* **2009**, *9*, 30–35. [CrossRef]
23. Li, X.; Cai, W.; An, J.; Kim, S.; Nah, J.; Yang, D.; Piner, R.; Velamakanni, A.; Jung, I.; Tutuc, E.; et al. Large-Area Synthesis of High-Quality and Uniform Graphene Films on Copper Foils. *Science* **2009**, *324*, 1312–1314. [CrossRef] [PubMed]
24. Shams, S.S.; Zhang, R.; Zhu, J. Graphene synthesis: A Review. *Mater. Sci.-Pol.* **2016**, *33*, 566–578. [CrossRef]
25. Muñoz, R.; Gómez-Aleixandre, C. Review of CVD Synthesis of Graphene. *Chem. Vap. Depos.* **2013**, *19*, 297–322. [CrossRef]
26. Emtsev, K.V.; Bostwick, A.; Horn, K.; Jobst, J.; Kellogg, G.L.; Ley, L.; McChesney, J.; Ohta, T.; Reshanov, S.A.; Röhrl, J.; et al. Towards wafer-size graphene layers by atmospheric pressure graphitization of silicon carbide. *Nat. Mater.* **2009**, *8*, 203–207. [CrossRef] [PubMed]
27. Zhang, R.; Dong, Y.; Kong, W.; Han, W.; Tan, P.-H.; Liao, Z.-M.; Wu, X.; Yu, D. Growth of large domain epitaxial graphene on the C-face of SiC. *J. Appl. Phys.* **2012**, *112*, 104307. [CrossRef]

28. Stankovich, S.; Dikin, D.A.; Piner, R.D.; Kohlhaas, K.A.; Kleinhammes, A.; Jia, Y.; Wu, Y.; Nguyen, S.; Ruoff, R.S. Synthesis of graphene-based nanosheets via chemical reduction of exfoliated graphite oxide. *Carbon* **2007**, *45*, 1558–1565. [CrossRef]
29. Schniepp, H.C.; Li, J.-L.; McAllister, M.J.; Sai, H.; Herrera-Alonso, M.; Adamson, D.H.; Prud'Homme, R.K.; Car, R.; Saville, D.A.; Aksay, I.A. Functionalized Single Graphene Sheets Derived from Splitting Graphite Oxide. *J. Phys. Chem. B* **2006**, *110*, 8535–8539. [CrossRef]
30. Park, S.; Ruoff, R.S. Chemical methods for the production of graphenes. *Nat. Nanotechnol.* **2009**, *4*, 217–224. [CrossRef]
31. Hummers, W.S.; Offeman, R.E. Preparation of Graphitic Oxide. *J. Am. Chem. Soc.* **1958**, *80*, 1339. [CrossRef]
32. Lawal, A.T. Graphene-based nano composites and their applications. A review. *Biosens. Bioelectron.* **2019**, *141*, 111384. [CrossRef] [PubMed]
33. Zhao, W.; Liu, H.; Meng, N.; Jian, M.; Wang, H.; Zhang, X. Graphene oxide incorporated thin film nanocomposite membrane at low concentration monomers. *J. Membr. Sci.* **2018**, *565*, 380–389. [CrossRef]
34. Akyüz, D.; Koca, A. Photocatalytic hydrogen production with reduced graphene oxide (RGO)-CdZnS nano-composites synthesized by solvothermal decomposition of dimethyl sulfoxide as the sulfur source. *J. Photochem. Photobiol. A Chem.* **2018**, *364*, 625–634. [CrossRef]
35. Kumar, N.; Rodriguez, J.R.; Pol, V.G.; Sen, A. Facile synthesis of 2D graphene oxide sheet enveloping ultrafine 1D LiMn2O4 as interconnected framework to enhance cathodic property for Li-ion battery. *Appl. Surf. Sci.* **2019**, *463*, 132–140. [CrossRef]
36. Aghazadeh, M. One-step Electrophoretic/electrochemical Synthesis of Reduced Graphene Oxide/Manganese Oxide (rGO-Mn3O4) Nanocomposite and Study of its Capacitive Performance. *Anal. Bioanal. Electrochem.* **2018**, *10*, 961–973.
37. Jasmi, F.; Azeman, N.H.; Bakar, A.A.A.; Zan, M.S.D.; Badri, K.H.; Su'ait, M.S. Ionic Conductive Polyurethane-Graphene Nanocomposite for Performance Enhancement of Optical Fiber Bragg Grating Temperature Sensor. *IEEE Access* **2018**, *6*, 47355–47363. [CrossRef]
38. Novoselov, K.S.; Geim, A.K.; Morozov, S.V.; Jiang, D.; Zhang, Y.; Dubonos, S.V.; Grigorieva, I.V.; Firsov, A.A. Electric Field Effect in Atomically Thin Carbon Films. *Science* **2004**, *306*, 666–669. [CrossRef]
39. Young, R.; Kinloch, I.A.; Gong, L.; Novoselov, K. The mechanics of graphene nanocomposites: A review. *Compos. Sci. Technol.* **2012**, *72*, 1459–1476. [CrossRef]
40. Lee, X.J.; Hiew, B.Y.Z.; Lai, K.C.; Lee, L.Y.; Gan, S.; Thangalazhy-Gopakumar, S.; Rigby, S. Review on graphene and its derivatives: Synthesis methods and potential industrial impleentation. *J. Taiwan Inst. Chem. Eng.* **2019**, *98*, 163–180. [CrossRef]
41. Hernandez, Y.; Nicolosi, V.; Lotya, M.; Blighe, F.M.; Sun, Z.; De, S.; McGovern, I.T.; Holland, B.; Byrne, M.; Gun'Ko, Y.; et al. High-yield production of graphene by liquid-phase exfoliation of graphite. *Nat. Nanotechnol.* **2008**, *3*, 563–568. [CrossRef]
42. Ciesielski, A.; Samorì, P. Graphene via sonication assisted liquid-phase exfoliation. *Chem. Soc. Rev.* **2014**, *43*, 381–398. [CrossRef]
43. Edwards, R.S.; Coleman, K.S. Graphene synthesis: Relationship to applications. *Nanoscale* **2013**, *5*, 38–51. [CrossRef] [PubMed]
44. Yi, M.; Shen, Z. A review on mechanical exfoliation for the scalable production of graphene. *J. Mater. Chem. A* **2015**, *3*, 11700–11715. [CrossRef]
45. Baig, Z.; Mamat, O.; Mustapha, M.; Mumtaz, A.; Munir, K.; Sarfraz, M. Investigation of tip sonication effects on structural quality of graphene nanoplatelets (GNPs) for superior solvent dispersion. *Ultrason. Sonochem.* **2018**, *45*, 133–149. [CrossRef] [PubMed]
46. Jiao, L.; Zhang, L.; Wang, X.; Diankov, G.; Dai, H. Narrow graphene nanoribbons from carbon nanotubes. *Nature* **2009**, *458*, 877–880. [CrossRef] [PubMed]
47. Kosynkin, D.V.; Higginbotham, A.L.; Sinitskii, A.; Lomeda, J.R.; Dimiev, A.; Price, B.K.; Tour, J. Longitudinal unzipping of carbon nanotubes to form graphene nanoribbons. *Nature* **2009**, *458*, 872–876. [CrossRef]
48. Cano-Márquez, A.G.; Rodriguez-Macias, F.; Campos-Delgado, J.; Espinosa-González, C.G.; Tristán-López, F.; Ramírez-González, D.; Cullen, D.; Smith, D.; Terrones, M.; Vega-Cantu, Y.I. Ex-MWNTs: Graphene Sheets and Ribbons Produced by Lithium Intercalation and Exfoliation of Carbon Nanotubes. *Nano Lett.* **2009**, *9*, 1527–1533. [CrossRef]
49. Thess, A.; Lee, R.; Nikolaev, P.; Dai, H.; Petit, P.; Robert, J.; Xu, C.; Lee, Y.H.; Kim, S.G.; Rinzler, A.G.; et al. Crystalline Ropes of Metallic Carbon Nanotubes. *Science* **1996**, *273*, 483–487. [CrossRef]
50. Liu, J.; Kim, G.-H.; Xue, Y.; Kim, J.Y.; Baek, J.-B.; Durstock, M.; Dai, L. Graphene Oxide Nanoribbon as Hole Extraction Layer to Enhance Efficiency and Stability of Polymer Solar Cells. *Adv. Mater.* **2013**, *26*, 786–790. [CrossRef]
51. Mahmoud, W.E.; Al-Hazmi, F.S.; Al-Harbi, G.H. Wall by wall controllable unzipping of MWCNTs via intercalation with oxalic acid to produce multilayers graphene oxide ribbon. *Chem. Eng. J.* **2015**, *281*, 192–198. [CrossRef]
52. Zhang, G.; Manjooran, N. Nanofabrication and its application in renewable energy. *Johns. Matthey Technol. Rev.* **2014**, *58*, 221–223.
53. Bhuyan, M.S.A.; Uddin, M.N.; Islam, M.M.; Bipasha, F.A.; Hossain, S.S. Synthesis of graphene. *Int. Nano Lett.* **2016**, *6*, 65–83. [CrossRef]
54. Arora, N.; Sharma, N.N. Arc discharge synthesis of carbon nanotubes: Comprehensive review. *Diam. Relat. Mater.* **2014**, *50*, 135–150. [CrossRef]
55. Li, Y.; Chen, Q.; Xu, K.; Kaneko, T.; Hatakeyama, R. Synthesis of graphene nanosheets from petroleum asphalt by pulsed arc discharge in water. *Chem. Eng. J.* **2013**, *215–216*, 45–49. [CrossRef]
56. Zhang, Y.; Zhang, L.; Zhou, C. Review of Chemical Vapor Deposition of Graphene and Related Applications. *Acc. Chem. Res.* **2013**, *46*, 2329–2339. [CrossRef] [PubMed]
57. Arjmandi-Tash, H.; Lebedev, N.; van Deursen, P.M.; Aarts, J.; Schneider, G.F. Hybrid cold and hot-wall reaction chamber for the rapid synthesis of uniform graphene. *Carbon* **2017**, *118*, 438–442. [CrossRef]

58. Cooper, D.R.; D'Anjou, B.; Ghattamaneni, N.; Harack, B.; Hilke, M.; Horth, A.; Majlis, N.; Massicotte, M.; Vandsburger, L.; Whiteway, E.; et al. Experimental Review of Graphene. *ISRN Condens. Matter Phys.* **2012**, *2012*, 501686. [CrossRef]
59. Mishra, N.; Boeckl, J.; Motta, N.; Iacopi, F. Graphene growth on silicon carbide: A review. *Phys. Status Solidi A* **2016**, *213*, 2277–2289. [CrossRef]
60. Cambaz, Z.G.; Yushin, G.; Osswald, S.; Mochalin, V.; Gogotsi, Y. Noncatalytic synthesis of carbon nanotubes, graphene and graphite on SiC. *Carbon* **2008**, *46*, 841–849. [CrossRef]
61. Brodie, B.C. Sur le poids atomique du graphite. *Ann. Chim. Phys.* **1860**, *59*, e472.
62. Staudenmaier, L. Verfahren zur Darstellung der Graphitsäure. *Eur. J. Inorg. Chem.* **1898**, *31*, 1481–1487. [CrossRef]
63. Hofmann, U.; König, E. Untersuchungen über graphitoxyd. *Chemie* **1937**, *234*, 311–336. [CrossRef]
64. Somanathan, T.; Prasad, K.; Ostrikov, K.; Saravanan, A.; Krishna, V.M. Graphene Oxide Synthesis from Agro Waste. *Nanomaterials* **2015**, *5*, 826–834. [CrossRef]
65. Yu, H.; Zhang, B.; Bulin, C.; Li, R.; Xing, R. High-efficient Synthesis of Graphene Oxide Based on Improved Hummers Method. *Sci. Rep.* **2016**, *6*, 36143. [CrossRef]
66. Chen, J.; Yao, B.; Li, C.; Shi, G. An improved Hummers method for eco-friendly synthesis of graphene oxide. *Carbon* **2013**, *64*, 225–229. [CrossRef]
67. Yoon, G.; Seo, D.-H.; Ku, K.; Kim, J.; Jeon, S.; Kang, K. Factors Affecting the Exfoliation of Graphite Intercalation Compounds for Graphene Synthesis. *Chem. Mater.* **2015**, *27*, 2067–2073. [CrossRef]
68. Konios, D.; Stylianakis, M.M.; Stratakis, E.; Kymakis, E. Dispersion behaviour of graphene oxide and reduced graphene oxide. *J. Colloid Interface Sci.* **2014**, *430*, 108–112. [CrossRef] [PubMed]
69. Chua, C.K.; Pumera, M. Chemical reduction of graphene oxide: A synthetic chemistry viewpoint. *Chem. Soc. Rev.* **2013**, *43*, 291–312. [CrossRef] [PubMed]
70. Kumar, P.V.; Bardhan, N.M.; Chen, G.-Y.; Li, Z.; Belcher, A.M.; Grossman, J.C. New insights into the thermal reduction of graphene oxide: Impact of oxygen clustering. *Carbon* **2016**, *100*, 90–98. [CrossRef]
71. Zheng, X.; Peng, Y.; Yang, Y.; Chen, J.; Tian, H.; Cui, X.; Zheng, W. Hydrothermal reduction of graphene oxide; effect on surface-enhanced Raman scattering. *J. Raman Spectrosc.* **2016**, *48*, 97–103. [CrossRef]
72. Chen, W.; Yan, L. Preparation of graphene by a low-temperature thermal reduction at atmosphere pressure. *Nanoscale* **2010**, *2*, 559–563. [CrossRef] [PubMed]
73. Yusuf, M.; Kumar, M.; Khan, M.A.; Sillanpää, M.; Arafat, H. A review on exfoliation, characterization, environmental and energy applications of graphene and graphene-based composites. *Adv. Colloid Interface Sci.* **2019**, *273*, 102036. [CrossRef] [PubMed]
74. Olabi, A.; Abdelkareem, M.A.; Wilberforce, T.; Sayed, E.T. Application of graphene in energy storage device–A review. *Renew. Sustain. Energy Rev.* **2020**, *135*, 110026. [CrossRef]
75. Zhao, X.; Li, H.; Han, F.; Dai, M.; Sun, Y.; Song, Z.; Han, D.; Niu, L. Electrochemical exfoliation of graphene as an anode material for ultra-long cycle lithium ion batteries. *J. Phys. Chem. Solids* **2019**, *139*, 109301. [CrossRef]
76. Ji, X.; Mu, Y.; Liang, J.; Jiang, T.; Zeng, J.; Lin, Z.; Lin, Y.; Yu, J. High yield production of 3D graphene powders by thermal chemical vapor deposition and application as highly efficient conductive additive of lithium ion battery electrodes. *Carbon* **2021**, *176*, 21–30. [CrossRef]
77. Folorunso, O.; Hamam, Y.; Sadiku, R.; Ray, S.S.; Adekoya, G.J. Investigation of graphene loaded polypyrrole for lithium-ion battery. *Mater. Today Proc.* **2020**, *38*, 635–638. [CrossRef]
78. Wu, Z.-S.; Ren, W.; Wen, L.; Gao, L.; Zhao, J.; Chen, Z.; Zhou, G.; Li, F.; Cheng, H.-M. Graphene Anchored with Co3O4 Nanoparticles as Anode of Lithium Ion Batteries with Enhanced Reversible Capacity and Cyclic Performance. *ACS Nano* **2010**, *4*, 3187–3194. [CrossRef]
79. Tian, R.; Zhang, Y.; Chen, Z.; Duan, H.; Xu, B.; Guo, Y.; Kang, H.; Li, H.; Liu, H. The effect of annealing on a 3D SnO2/graphene foam as an advanced lithium-ion battery anode. *Sci. Rep.* **2016**, *6*, 19195. [CrossRef]
80. Wang, D.; Choi, D.; Li, J.; Yang, Z.; Nie, Z.; Kou, R.; Hu, D.; Wang, C.; Saraf, L.V.; Zhang, J.; et al. Self-Assembled TiO_2–Graphene Hybrid Nanostructures for Enhanced Li-Ion Insertion. *ACS Nano* **2009**, *3*, 907–914. [CrossRef]
81. Idrees, M.; Batool, S.; Kong, J.; Zhuang, Q.; Liu, H.; Shao, Q.; Lu, N.; Feng, Y.; Wujcik, E.K.; Gao, Q.; et al. Polyborosilazane derived ceramics-nitrogen sulfur dual doped graphene nanocomposite anode for enhanced lithium ion batteries. *Electrochim. Acta* **2019**, *296*, 925–937. [CrossRef]
82. Lee, S.J.; Theerthagiri, J.; Nithyadharseni, P.; Arunachalam, P.; Balaji, D.; Kumar, A.M.; Madhavan, J.; Mittal, V.; Choi, M.Y. Heteroatom-doped graphene-based materials for sustainable energy applications: A review. *Renew. Sustain. Energy Rev.* **2021**, *143*, 110849. [CrossRef]
83. Reddy, A.L.M.; Srivastava, A.; Gowda, S.R.; Gullapalli, H.; Dubey, M.; Ajayan, P.M. Synthesis of Nitrogen-Doped Graphene Films For Lithium Battery Application. *ACS Nano* **2010**, *4*, 6337–6342. [CrossRef] [PubMed]
84. Wang, H.; Zhang, C.; Liu, Z.; Wang, L.; Han, P.; Xu, H.; Zhang, K.; Dong, S.; Yao, J.; Cui, G. Nitrogen-doped graphene nanosheets with excellent lithium storage properties. *J. Mater. Chem.* **2011**, *21*, 5430–5434. [CrossRef]
85. Yang, J.; Jia, K.; Wang, M.; Liu, S.; Hu, C.; Zhang, K.; Zhang, Y.; Qiu, J. Fabrication of nitrogen-doped porous graphene hybrid nanosheets from metal–organic frameworks for lithium-ion batteries. *Nanotechnology* **2019**, *31*, 145402. [CrossRef]
86. Wu, Z.-S.; Ren, W.; Xu, L.; Li, F.; Cheng, H.-M. Doped Graphene Sheets as Anode Materials with Superhigh Rate and Large Capacity for Lithium Ion Batteries. *ACS Nano* **2011**, *5*, 5463–5471. [CrossRef]

87. Paek, S.-M.; Yoo, E.; Honma, I. Enhanced cyclic performance and lithium storage capacity of SnO_2/graphene nanoporous electrodes with three-dimensionally delaminated flexible structure. *Nano Lett.* **2009**, *9*, 72–75. [CrossRef] [PubMed]
88. Wu, Z.-S.; Wang, D.-W.; Ren, W.; Zhao, J.; Zhou, G.; Li, F.; Cheng, H.-M. Anchoring Hydrous RuO_2 on Graphene Sheets for High-Performance Electrochemical Capacitors. *Adv. Funct. Mater.* **2010**, *20*, 3595–3602. [CrossRef]
89. Zheng, F.; Yang, Y.; Chen, Q. High lithium anodic performance of highly nitrogen-doped porous carbon prepared from a metal-organic framework. *Nat. Commun.* **2014**, *5*, 5261. [CrossRef]
90. Zhu, Y.; Li, L.; Zhang, C.; Casillas, G.; Sun, Z.; Yan, Z.; Ruan, G.; Peng, Z.; Raji, A.-R.; Kittrell, C.; et al. A seamless three-dimensional carbon nanotube graphene hybrid material. *Nat. Commun.* **2012**, *3*, 1225. [CrossRef]
91. Yan, Z.; Ma, L.; Zhu, Y.; Lahiri, I.; Hahm, M.G.; Liu, Z.; Yang, S.; Xiang, C.; Lu, W.; Peng, Z.J.A. Three-dimensional metal–graphene–nanotube multifunctional hybrid materials. *ACS Nano* **2013**, *7*, 58–64. [CrossRef]
92. Xing, L.L.; Wu, X.; Huang, K.J. High-performance supercapacitor based on three-dimensional flower-shaped $Li_4Ti_5O_{12}$-graphene hybrid and pine needles derived honeycomb carbon. *J. Colloid Interface Sci.* **2018**, *529*, 171–179. [CrossRef] [PubMed]
93. Wang, H.; Tran, D.; Moussa, M.; Stanley, N.; Tung, T.T.; Yu, L.; Yap, P.L.; Ding, F.; Qian, J.; Losic, D. Improved preparation of MoS_2/graphene composites and their inks for supercapacitors applications. *Mater. Sci. Eng. B* **2020**, *262*, 114700. [CrossRef]
94. Chen, Z.; Zhao, S.; Zhao, H.; Zou, Y.; Yu, C.; Zhong, W. Nitrogen-doped interpenetrating porous carbon/graphene networks for supercapacitor applications. *Chem. Eng. J.* **2020**, *409*, 127891. [CrossRef]
95. Gopakumar, D.A.; Arumughan, V.; Pottathara, Y.B.; Sisant, S.K.; Pasquini, D.; Bračič, M.; Seantier, B.; Nzihou, A.; Thomas, S.; Rizal, S.; et al. Robust Superhydrophobic Cellulose Nanofiber Aerogel for Multifunctional Environmental Applications. *Polymers* **2019**, *11*, 495. [CrossRef]
96. Pottathara, Y.B.; Tiyyagura, H.R.; Ahmad, Z.; Sadasivuni, K.K. Graphene based aerogels: Fundamentals and applications as supercapacitors. *J. Energy Storage* **2020**, *30*, 101549. [CrossRef]
97. Zhang, L.; Chen, H.; Lu, X.; Wang, Y.; Tan, L.; Sui, D.; Qi, W. Fabrication of N, S co-doped graphene aerogel for high-performance supercapacitors: π-conjugated planar molecules as efficient dopants and pillared agents. *Appl. Surf. Sci.* **2020**, *529*, 147022. [CrossRef]
98. Arkhipova, E.A.; Ivanov, A.S.; Maslakov, K.I.; Egorov, A.V.; Savilov, S.V.; Lunin, V.V. Mesoporous graphene nanoflakes for high performance supercapacitors with ionic liquid electrolyte. *Microporous Mesoporous Mater.* **2019**, *294*, 109851. [CrossRef]
99. Schedin, F.; Geim, A.K.; Morozov, S.V.; Hill, E.W.; Blake, P.; Katsnelson, M.I.; Novoselov, K.S. Detection of individual gas molecules adsorbed on graphene. *Nat. Mater.* **2007**, *6*, 652–655. [CrossRef]
100. Novoselov, K.; Geim, A.K.; Morozov, S.; Jiang, D.; Katsnelson, M.I.; Grigorieva, I.V.; Dubonos, S.V.; Firsov, A.A. Two-dimensional gas of massless Dirac fermions in graphene. *Nature* **2005**, *438*, 197–200. [CrossRef]
101. Novoselov, K.S.; Jiang, Z.; Zhang, Y.; Morozov, S.V.; Stormer, H.L.; Zeitler, U.; Maan, J.C.; Boebinger, G.S.; Kim, P.; Geim, A.K. Room-Temperature Quantum Hall Effect in Graphene. *Science* **2007**, *315*, 1379. [CrossRef]
102. Fowler, J.D.; Allen, M.J.; Tung, V.; Yang, Y.; Kaner, R.B.; Weiller, B.H. Practical Chemical Sensors from Chemically Derived Graphene. *ACS Nano* **2009**, *3*, 301–306. [CrossRef] [PubMed]
103. Sundaram, R.S.; Gómez-Navarro, C.; Balasubramanian, K.; Burghard, M.; Kern, K.J.A.M. Electrochemical modification of graphene. *Adv. Mater.* **2008**, *20*, 3050–3053. [CrossRef]
104. Gupta, S.; Meek, R. Metal nanoparticles-grafted functionalized graphene coated with nanostructured polyaniline 'hybrid' nanocomposites as high-performance biosensors. *Sens. Actuators B Chem.* **2018**, *274*, 85–101. [CrossRef]
105. Shan, C.; Yang, H.; Song, J.; Han, D.; Ivaska, A.; Niu, L. Direct electrochemistry of glucose oxidase and biosensing for glucose based on graphene. *Anal. Chem.* **2009**, *81*, 2378–2382. [CrossRef]
106. Kang, X.; Wang, J.; Wu, H.; Aksay, I.A.; Liu, J.; Lin, Y. Glucose oxidase–graphene–chitosan modified electrode for direct electrochemistry and glucose sensing. *Biosens. Bioelectron.* **2009**, *25*, 901–905. [CrossRef] [PubMed]
107. Liu, Y.; Wang, M.; Zhao, F.; Xu, Z.; Dong, S. The direct electron transfer of glucose oxidase and glucose biosensor based on carbon nanotubes/chitosan matrix. *Biosens. Bioelectron.* **2005**, *21*, 984–988. [CrossRef]
108. Liu, S.; Ju, H. Reagentless glucose biosensor based on direct electron transfer of glucose oxidase immobilized on colloidal gold modified carbon paste electrode. *Biosens. Bioelectron.* **2003**, *19*, 177–183. [CrossRef]
109. Huang, Y.; Zhang, W.; Xiao, H.; Li, G. An electrochemical investigation of glucose oxidase at a CdS nanoparticles modified electrode. *Biosens. Bioelectron.* **2005**, *21*, 817–821. [CrossRef]
110. Wu, H.; Wang, J.; Kang, X.; Wang, C.; Wang, D.; Liu, J.; Aksay, I.A.; Lin, Y.J.T. Glucose biosensor based on immobilization of glucose oxidase in platinum nanoparticles/graphene/chitosan nanocomposite film. *Talanta* **2009**, *80*, 403–406. [CrossRef]
111. Liu, H.; Gao, J.; Xue, M.; Zhu, N.; Zhang, M.; Cao, T.J.L. Processing of graphene for electrochemical application: Noncovalently functionalize graphene sheets with water-soluble electroactive methylene green. *Langmuir* **2009**, *25*, 12006–12010. [CrossRef]
112. Sassolas, A.; Leca-Bouvier, B.; Blum, L.J. DNA Biosensors and Microarrays. *Chem. Rev.* **2007**, *108*, 109–139. [CrossRef]
113. Drummond, T.G.; Hill, M.G.; Barton, J.K. Electrochemical DNA sensors. *Nat. Biotechnol.* **2003**, *21*, 1192–1199. [CrossRef] [PubMed]
114. Ohno, Y.; Maehashi, K.; Matsumoto, K. Label-Free Biosensors Based on Aptamer-Modified Graphene Field-Effect Transistors. *J. Am. Chem. Soc.* **2010**, *132*, 18012–18013. [CrossRef]
115. Kybert, N.J.; Han, G.H.; Lerner, M.B.; Dattoli, E.N.; Esfandiar, A.; Johnson, A.T.C. Scalable arrays of chemical vapor sensors based on DNA-decorated graphene. *Nano Res.* **2013**, *7*, 95–103. [CrossRef]

116. Zhou, M.; Zhai, Y.; Dong, S. Electrochemical Sensing and Biosensing Platform Based on Chemically Reduced Graphene Oxide. *Anal. Chem.* **2009**, *81*, 5603–5613. [CrossRef] [PubMed]
117. Green, N.S.; Norton, M.L. Interactions of DNA with graphene and sensing applications of graphene field-effect transistor devices: A review. *Anal. Chim. Acta* **2015**, *853*, 127–142. [CrossRef] [PubMed]
118. Dong, X.; Shi, Y.; Huang, W.; Chen, P.; Li, L.-J. Electrical Detection of DNA Hybridization with Single-Base Specificity Using Transistors Based on CVD-Grown Graphene Sheets. *Adv. Mater.* **2010**, *22*, 1649–1653. [CrossRef]
119. Li, J.; Guo, S.; Zhai, Y.; Wang, E. High-sensitivity determination of lead and cadmium based on the Nafion-graphene composite film. *Anal. Chim. Acta* **2009**, *649*, 196–201. [CrossRef]
120. Li, J.; Guo, S.; Zhai, Y.; Wang, E.J.E.C. Nafion–graphene nanocomposite film as enhanced sensing platform for ultrasensitive determination of cadmium. *Electrochem. Commun.* **2009**, *11*, 1085–1088. [CrossRef]
121. Kefala, G.; Economou, A.; Voulgaropoulos, A. A study of Nafion-coated bismuth-film electrodes for the determination of trace metals by anodic stripping voltammetry. *Analyst* **2004**, *129*, 1082–1090. [CrossRef]
122. Liu, B.; Lu, L.; Wang, M.; Zi, Y. A Study of Nafion-Coated Bismuth-Film Electrode for the Determination of Zinc, Lead, and Cadmium in Blood Samples. *Electroanalysis* **2008**, *20*, 2363–2369. [CrossRef]
123. Choi, W.-J.; Kwak, D.-J.; Park, C.-S.; Sung, Y.-M. Characterization of Transparent Conductive ITO, ITiO, and FTO Films for Application in Photoelectrochemical Cells. *J. Nanosci. Nanotechnol.* **2012**, *12*, 3394–3397. [CrossRef] [PubMed]
124. Kim, K.S.; Zhao, Y.; Jang, H.; Lee, S.Y.; Kim, J.M.; Kim, K.S.; Ahn, J.-H.; Kim, P.; Choi, J.-Y.; Hong, B.H. Large-scale pattern growth of graphene films for stretchable transparent electrodes. *Nature* **2009**, *457*, 706–710. [CrossRef] [PubMed]
125. Wang, X.; Zhi, L.; Müllen, K. Transparent, Conductive Graphene Electrodes for Dye-Sensitized Solar Cells. *Nano Lett.* **2007**, *8*, 323–327. [CrossRef] [PubMed]
126. Hong, W.; Xu, Y.; Lu, G.; Li, C.; Shi, G. Transparent graphene/PEDOT–PSS composite films as counter electrodes of dye-sensitized solar cells. *Electrochem. Commun.* **2008**, *10*, 1555–1558. [CrossRef]
127. Kang, J.H.; Choi, S.; Park, Y.J.; Park, J.S.; Cho, N.S.; Cho, S.; Walker, B.; Choi, D.S.; Shin, J.-W.; Seo, J.H. Cu/graphene hybrid transparent conducting electrodes for organic photovoltaic devices. *Carbon* **2020**, *171*, 341–349. [CrossRef]
128. Huang, C.-H.; Wu, H.-C.; Chen, B.-F.; Li, Y.-C. Graphene/Silver Nanowires/Graphene Sandwich Composite for Stretchable Transparent Electrodes and Its Fracture Mechanism. *Micromachines* **2021**, *12*, 512. [CrossRef]
129. Ren, X.; Chen, C.; Nagatsu, M.; Wang, X. Carbon nanotubes as adsorbents in environmental pollution management: A review. *Chem. Eng. J.* **2011**, *170*, 395–410. [CrossRef]
130. Sitko, R.; Zawisza, B.; Malicka, E. Graphene as a new sorbent in analytical chemistry. *TrAC Trends Anal. Chem.* **2013**, *51*, 33–43. [CrossRef]
131. Yao, Y.; Yang, Z.; Zhang, D.; Peng, W.; Sun, H.; Wang, S. Magnetic $CoFe_2O_4$–graphene hybrids: Facile synthesis, characterization, and catalytic properties. *Ind. Eng. Chem. Res.* **2012**, *51*, 6044–6051. [CrossRef]
132. Zhu, J.; Wei, S.; Gu, H.; Rapole, S.B.; Wang, Q.; Luo, Z.; Haldolaarachchige, N.; Young, D.P.; Guo, Z. One-Pot Synthesis of Magnetic Graphene Nanocomposites Decorated with Core@Double-shell Nanoparticles for Fast Chromium Removal. *Environ. Sci. Technol.* **2011**, *46*, 977–985. [CrossRef]
133. Liu, M.; Chen, C.; Hu, J.; Wu, X.; Wang, X. Synthesis of magnetite/graphene oxide composite and application for cobalt (II) removal. *J. Phys. Chem. C* **2011**, *115*, 25234–25240. [CrossRef]
134. Ghosh, A.; Subrahmanyam, K.S.; Krishna, K.S.; Datta, S.; Govindaraj, A.; Pati, S.K.; Rao, C.N.R. Uptake of H_2 and CO_2 by Graphene. *J. Phys. Chem. C* **2008**, *112*, 15704–15707. [CrossRef]
135. Liu, Y.; Wilcox, J. CO_2 Adsorption on Carbon Models of Organic Constituents of Gas Shale and Coal. *Environ. Sci. Technol.* **2010**, *45*, 809–814. [CrossRef] [PubMed]
136. Liu, Y.; Wilcox, J. Molecular Simulation Studies of CO_2 Adsorption by Carbon Model Compounds for Carbon Capture and Sequestration Applications. *Environ. Sci. Technol.* **2012**, *47*, 95–101. [CrossRef] [PubMed]
137. Perera, S.; Mariano, R.; Vu, K.; Nour, N.; Seitz, O.; Chabal, Y.; Balkus, K. Hydrothermal synthesis of graphene-TiO_2 nanotube composites with enhanced photocatalytic activity. *ACS Catal.* **2012**, *2*, 949–956. [CrossRef]
138. Zhang, H.; Lv, X.; Li, Y.; Wang, Y.; Li, J. P25-Graphene Composite as a High Performance Photocatalyst. *ACS Nano* **2010**, *4*, 380–386. [CrossRef]
139. Liu, J.; Bai, H.; Wang, Y.; Liu, Z.; Zhang, X.; Sun, D.D. Self-Assembling TiO_2 Nanorods on Large Graphene Oxide Sheets at a Two-Phase Interface and Their Anti-Recombination in Photocatalytic Applications. *Adv. Funct. Mater.* **2010**, *20*, 4175–4181. [CrossRef]